electronics

MDPI

Article

Enhancing Medical Image Denoising: A Hybrid Approach Incorporating Adaptive Kalman Filter and Non-Local Means with Latin Square Optimization

Mehdi Taassori [1,*] and Béla Vizvári [2]

[1] Institute of Cyberphysical Systems, John von Neumann Faculty of Informatics, Obuda University, 1034 Budapest, Hungary
[2] Department of Industrial Engineering, Eastern Mediterranean University, Famagusta 99628, Cyprus; bela.vizvari@emu.edu.tr
* Correspondence: taassori.mehdi@uni-obuda.hu

Abstract: Medical image denoising plays a critical role in enhancing the quality of diagnostic imaging, where noise reduction without compromising image details is paramount. In this paper, we propose a novel hybrid approach aimed at improving the denoising efficacy for medical images. Initially, we employ an adaptive Kalman filter to attenuate noise, leveraging its proficiency in state estimation from noisy measurements. Unlike conventional Kalman filters with fixed parameters, our adaptive Kalman filter dynamically adjusts its parameters based on the noise characteristics of the input image, thus offering enhanced accuracy in estimating the underlying true state of the system represented by the medical image. Subsequently, both a non-local means (NLM) method and a median filter are introduced as post-processing steps to further refine the denoised image. The NLM method leverages the similarities between image patches to effectively reduce noise, while the median filter further enhances the denoised image by suppressing residual noise and preserving image details. However, the effectiveness of NLM and the median filter is highly dependent on carefully chosen parameters, which traditionally necessitates extensive computational resources for optimization. To address this challenge, we introduce the innovative use of Latin square optimization, a structured experimental design technique, to efficiently determine optimal parameters for NLM. By systematically exploring parameter combinations using Latin square optimization, we mitigate the complexity of experiments while enhancing denoising performance. The experimental results on medical images demonstrate the effectiveness of our proposed approach, showcasing significant improvements in noise reduction and the preservation of image features compared to conventional methods. Our hybrid approach not only advances the state-of-the-art in medical image denoising but also presents a practical solution for optimizing parameter selection in NLM, thereby facilitating their broader adoption in medical imaging applications.

Keywords: Kalman filters; non-local means; Latin square; denoising; medical imaging

check for updates

Citation: Taassori, M.; Vizvári, B. Enhancing Medical Image Denoising: A Hybrid Approach Incorporating Adaptive Kalman Filter and Non-Local Means with Latin Square Optimization. *Electronics* **2024**, *13*, 2640. https://doi.org/10.3390/electronics13132640

Academic Editor: Maria Filomena Santarelli

Received: 10 June 2024
Revised: 28 June 2024
Accepted: 1 July 2024
Published: 5 July 2024

Copyright: © 2024 by the authors. Licensee MDPI, Basel, Switzerland. This article is an open access article distributed under the terms and conditions of the Creative Commons Attribution (CC BY) license (https://creativecommons.org/licenses/by/4.0/).

1. Introduction

In the realm of image processing, the task of denoising holds significance. Images captured in real-world scenarios are often damaged by various forms of noise, stemming from sources such as sensor imperfections, transmission errors, or environmental factors. The development of effective denoising techniques is crucial to enhance the utility of images across numerous applications. In the field of image processing, numerous researchers have employed diverse denoising methods to address Gaussian noise [1–8]. These approaches encompass a range of techniques appropriate to effectively remove noise while preserving important image features. Through extensive experimentation and analysis, researchers have aimed to identify the most suitable denoising strategy for specific applications. The researchers in [9–12] utilized noise modeling and parameter estimation techniques to

effectively remove noise from images. In [13], the authors introduced a prior learning-based method, which bypasses the challenges posed by noise modeling techniques. Specifically, it leverages external prior learning to direct its internal prior learning. Due to its strong prior modeling capability, their method demonstrates high effectiveness and robustness in handling real noisy images featuring realistic objects within complex scenes. However, a significant drawback still persists. The issues they address primarily center on learning image priors, which are predominantly defined based on human knowledge.

The Kalman filter (KF) is a widely used algorithm for estimating the current states of a system over time based on input measurements and a mathematical process model. However, its application to nonlinear systems can be challenging, prompting the development of the extended Kalman filter (EKF) and unscented Kalman filter (UKF) as alternatives for handling nonlinearity. Additionally, recent research has focused on Multiple Model (MM) filters, such as the Multiple Model Adaptive Estimation (MMAE) and Interacting Multiple Model (IMM) methods, which offer improved reliability by employing multiple filters with different models in parallel [14].

The unscented Kalman filter, an extension of the traditional Kalman filter, has found application in image processing tasks [15,16]. The researchers in [15] offered a straightforward yet powerful solution for real-world image denoising by combining deep neural networks with the unscented Kalman filter, presenting a promising approach to address this challenging problem. In [17], the researchers introduced a Kalman filter framework for signal denoising, which combines conventional linear time-invariant filtering with total variation denoising concurrently. The authors in [18] introduced a novel feature-preserving non-local means approach for denoising fluorescence images of live cells, improving feature recovery and particle detection. The impact of different center weights on the performance of the non-local means (NLM) method in image denoising, proposing a two-step non-local means (TSNLM) iterative scheme to mitigate issues such as insufficient denoising, is suggested in [19]. The proposed multiple-reconstruction NLM filtering (MR-NLM) [20] leverages redundant information from various reconstructions of PET (or SPECT) imaging data, termed auxiliary images, to effectively denoise target images contaminated with different noise levels or properties, enhancing the robustness of denoising in medical imaging applications. In [21], the authors' proposed denoising framework for brain PET images combines multi-scale transform (wavelet and curvelet) with tree clustering non-local means (TNLM) to effectively address challenges in noise removal and ROI segmentation, achieving better performance compared to existing methods, particularly in preserving edges and enhancing contrast. In [22], the authors introduced a novel non-local means-based framework (NMF) for mixed noise removal in images, utilizing a median-type filter to detect outlier pixels and replace them with their non-local means, approximating the complex noise distribution to Gaussian. Additionally, a low rank approximation combined with NMF (LRNM) model is proposed, incorporating gradient regularization for better texture preservation, and a convolutional neural network (CNN) combined with NMF (NMFCNN) is presented, demonstrating strong mixed noise removal performance and visually pleasing denoising results. The researchers in [23] investigated the significance of noise reduction in image processing applications. This study aims to address this challenge by employing the Kalman filter. The focus lies on constructing an image model based on Markov random fields and integrating the Kalman filter as a smoother to minimize noise effectively. In [24], the authors addressed the challenge of image noise in video processing, originating from various sources such as acquisition, transfer, and image compression. The proposed solution is a real-time video denoising algorithm that combines the Kalman and Bilateral filters. The key focus of the suggested method lies in not only attenuating noise but also ensuring a low computational cost, thus rendering it suitable for real-time applications.

In this study, we propose a comprehensive approach for enhancing medical image denoising, integrating adaptive Kalman filtering with non-local means and median filtering as post-processing steps, and employing Latin square optimization to optimize parameters for the non-local means algorithm. The adaptive Kalman filter serves as the foundation

of our denoising strategy, dynamically adjusting its parameters based on the noise characteristics of the input image. This adaptability ensures precise noise reduction while preserving crucial image features. Following Kalman filtering, we introduce non-local means and median filtering to further refine the denoised image. However, selecting optimal parameters for these techniques can be challenging, often requiring extensive computational resources. To address this challenge, we employ Latin square optimization, a structured experimental design technique, to efficiently determine the best parameters for the non-local means method. By systematically exploring parameter combinations using Latin square optimization, we enhance denoising performance while mitigating the complexity of experiments. The rest of this paper is structured as follows. Motivation is described in Section 2. In Section 3, our primary focus is on introducing the proposed method. In Section 4, the central focus is on presenting the experimental results. Finally, in Section 5, we conclude this paper.

2. Motivation

Medical imaging serves as a foundation in modern healthcare, facilitating the accurate diagnosis and treatment of a wide array of medical conditions. However, the efficacy of medical image interpretation is contingent upon the quality of the images obtained. Image noise, originating from various sources including equipment limitations, patient movement, and electronic interference, poses a significant obstacle in the pursuit for clear and informative medical images. The consequences of image noise in medical imaging are profound. Noise can conceal critical anatomical structures, distort pathological findings, and introduce artifacts that may lead to misdiagnosis or improper treatment decisions. Particularly in diagnostic modalities such as MRI, CT, and ultrasound, the presence of noise can compromise diagnostic accuracy and impede the clinician's ability to make informed decisions.

Traditional denoising techniques, such as Gaussian filtering and median filtering, have been employed to mitigate image noise. However, these methods often apply fixed parameters for noise reduction, which may not be optimal for all images or noise profiles. Moreover, while these techniques may effectively suppress noise, they may also inadvertently blur or distort important image features, diminishing the diagnostic value of the image. The imperative to enhance medical image denoising arises from the need to overcome these limitations and improve the diagnostic utility of medical images. By developing advanced denoising strategies that can effectively remove noise while preserving crucial image details, we can empower clinicians with clearer, more informative images that enhance diagnostic confidence and improve patient outcomes.

As mentioned, traditional methods apply fixed parameters for noise reduction, which may not be optimal for all images. Kalman filtering, a recursive estimation algorithm, has shown promise in adaptive noise reduction by dynamically adjusting filtering parameters based on the noise characteristics of the input image. Using an adaptive denoising technique such as the adaptive Kalman filter offers distinct advantages over traditional fixed-parameter methods. The adaptability of the adaptive Kalman filter allows for real-time adjustments of filtering parameters based on the specific noise characteristics of each medical image. This dynamic approach ensures that the denoising process is finely tuned to preserve critical image features while effectively reducing noise. Unlike fixed-parameter methods, which may oversimplify the noise reduction process and compromise image quality, the adaptive Kalman filter provides a tailored solution that can accommodate the inherent variability in medical imaging data. By leveraging the adaptive capabilities of the adaptive Kalman filter, our denoising approach aims to achieve superior results in terms of both noise reduction and image preservation. Additionally, the adaptive nature of the adaptive Kalman filter enhances its versatility across different imaging modalities and clinical scenarios, making it a valuable tool in the medical imaging toolkit.

However, applying Kalman filtering alone may not suffice for the complex noise patterns encountered in medical images. Non-local means filtering is a powerful denoising

technique that operates on the principle of exploiting redundancy in image information. Unlike traditional filtering methods that rely solely on local pixel neighborhoods, non-local means filtering considers similarities between patches of pixels across the entire image. By averaging pixel intensities weighted by the similarity between patches, non-local means filtering effectively preserves image structures while reducing noise. Nevertheless, selecting optimal parameters for non-local means filtering can be challenging due to several reasons:

1. Complexity of Image Structures: Images often contain a diverse range of structures, textures, and patterns. Determining the appropriate parameters for non-local means filtering requires considering the scale and characteristics of these structures, which can vary significantly across different images and imaging modalities.
2. Trade-off between Denoising and Detail Preservation: Non-local means filtering aims to strike a balance between denoising and preserving important image details. Selecting optimal parameters involves finding the right balance between noise reduction and maintaining image sharpness and clarity.
3. Computational Complexity: Non-local means filtering involves comparing patches of pixels across the entire image, which can be computationally intensive, particularly for high-resolution images. Selecting optimal parameters that achieve satisfactory denoising results while minimizing computational overhead is essential for practical applications.
4. Impact of Noise Characteristics: The effectiveness of non-local means filtering can vary depending on the characteristics of the noise present in the image. Selecting parameters that are adaptive to different noise profiles and levels is crucial for achieving optimal denoising performance.

Overall, while non-local means filtering offers significant advantages in terms of preserving image structures and achieving effective denoising, selecting optimal parameters requires careful consideration of various factors such as image content, noise characteristics, and computational efficiency. Advanced optimization techniques, such as Latin square optimization, can help streamline this parameter selection process and enhance the overall performance of non-local means filtering in medical image denoising.

In recent years, numerous image encryption schemes have emerged utilizing Latin squares. In [25], a new image encryption algorithm is introduced, departing from the conventional 2D Freidrich architecture and instead leveraging Latin square arrays. The proposed approach employs two Latin square matrices for the scrambling and diffusion of image data along both rows and columns. Notably, the encryption process involves sequential scrambling and diffusion operations, ensuring that each row and column undergoes encryption before the process concludes. In general, when the Latin squares are applied to encrypting color images, these algorithms typically treat each color channel separately, neglecting the intrinsic relationships between the color image and Latin squares. Consequently, such approaches often involve redundant operations and exhibit low efficiency. To overcome these limitations, the authors in [26] presented a new Color Image Encryption Algorithm (CIEA) that takes into account the specific properties of both color images and Latin squares. Initially, they introduce a two-dimensional chaotic system designed to address the shortcomings observed in existing chaotic systems. Subsequently, leveraging orthogonal Latin squares, they develop the proposed CIEA, which capitalizes on the inherent connections between orthogonal Latin squares and color images. Notably, the encryption process is conducted at the pixel level, ensuring a comprehensive integration of color image characteristics and Latin square properties. To enable real-time image encryption, the researchers in [27] proposed a fast color image encryption scheme that combines 3D orthogonal Latin squares (3D-OLSs) with a matching matrix. The 3D-OLSs ensure that each plane of two matrices adheres to the Latin square property, with corresponding planes satisfying orthogonality. Additionally, a matching matrix is introduced to generate an orthogonal matrix with the 3D Latin square. A novel 3D permutation method, utilizing 3D-OLSs and the matching matrix, is devised to streamline the permutation process, sig-

nificantly reducing the encryption time as orthogonal Latin squares are directly defined over integers.

3. Proposed Method

In this section, we present our novel approach for enhancing the denoising of medical images through the integration of the Kalman filter and non-local means (NLM) algorithm, followed by a post-processing step leveraging NLM.

3.1. Kalman Filter for Noise Attenuation

The Kalman filter is a powerful tool commonly used in signal processing for state estimation in dynamic systems. In the context of image denoising, the Kalman filter serves as an initial step to reduce noise while retaining the essential structural features of images. Its effectiveness lies in its ability to iteratively estimate the true state of the image from noisy measurements. In the context of medical image denoising, the Kalman filter serves as the initial step in our denoising pipeline.

3.2. Adaptive Kalman Filter

The motivation for adaptive Kalman filtering lies in addressing the limitations of traditional fixed-parameter Kalman filtering techniques when dealing with image denoising. Traditional Kalman filters assume fixed parameters for the measurement noise covariance and process noise covariance matrices, which may not effectively capture the varying characteristics of noise present in different images or the regions within an image. This limitation becomes particularly evident in scenarios where the noise level fluctuates significantly across different parts of an image. Let us explore why adaptive Kalman filtering offers a compelling solution for enhancing denoising performance.

- Dynamic Nature of Image Noise:

Image noise is often non-uniform and exhibits spatial variation, depending on factors such as imaging conditions, sensor characteristics, and environmental factors. Fixed-parameter Kalman filters are not inherently capable of adapting to these variations and may yield suboptimal results when applied to images with noise distributions.

- Optimizing Denoising Performance:

The goal of image denoising is to minimize the distortion caused by noise while preserving important image features. Adaptive techniques, such as adaptive Kalman filtering, aim to dynamically adjust filtering parameters to better match the characteristics of the noise present in the input image.

- Robustness to Changing Environments:

In real-world applications, imaging conditions and noise characteristics may change over time or across different scenarios. Adaptive filtering techniques, including adaptive Kalman filtering, offer increased robustness by continuously adjusting filter parameters based on the observed noise level, ensuring optimal performance in varying environments.

In the proposed adaptive Kalman filter method for image denoising, the filter parameters are dynamically adjusted based on the noise level present in the image. The adaptive nature of the method lies in the estimation and incorporation of the noise standard deviation into the Kalman filter's measurement and process noise covariances. This adaptation ensures that the filter adapts to varying noise levels across different regions of the image. The effectiveness of the proposed method is demonstrated through iterative denoising, where the Kalman filter is iteratively applied alongside adaptive filtering and post-processing techniques such as non-local means denoising and median filtering. To enhance the adaptability of the Kalman filter for diverse medical images and fluctuating noise levels, leverage statistical measures such as the standard deviation of noise. Dynamically adjusting parameters like measurement noise covariance and process noise covariance based on these measures enables the adaptive Kalman filter to effectively customize its

performance to different image characteristics and noise profiles. The adaptive Kalman filter demonstrates robustness in handling diverse noise patterns and variations in initial image quality. Its dynamic parameter adjustment based on observed data enables the effective reduction in various noise types commonly encountered in medical imaging, including Gaussian and Poisson noise.

The Kalman filter operates with two main stages: Prediction and Update.

- Prediction:

$$\hat{x}_{k|k-1} = A\hat{x}_{k-1|k-1} + Bu_{k-1}$$

$$P_{k|k-1} = AP_{k-1|k-1}A^T + Q_{k-1}$$

where $\hat{x}_{k|k-1}$ is the predicted state estimate at time k given the estimate at time $k-1$, $P_{k|k-1}$ is the predicted estimate covariance, A is the state transition matrix, B is the control input matrix, u_{k-1} is the control input, and Q is the process noise covariance.

- Update:

$$K_k = P_{k|k-1}H^T\left(HP_{k|k-1}H^T + R\right)^{-1}$$

$$\hat{x}_{k|k} = \hat{x}_{k|k-1} + K_k\left(z_k - H\hat{x}_{k|k-1}\right)$$

$$P_{k|k} = (I - K_kH)P_{k|k-1}$$

where K_k is the Kalman gain, z_k is the measurement at time k, H is the measurement matrix, and R is the measurement noise covariance. Figure 1 provides a comprehensive depiction of the Kalman filter's operation [28].

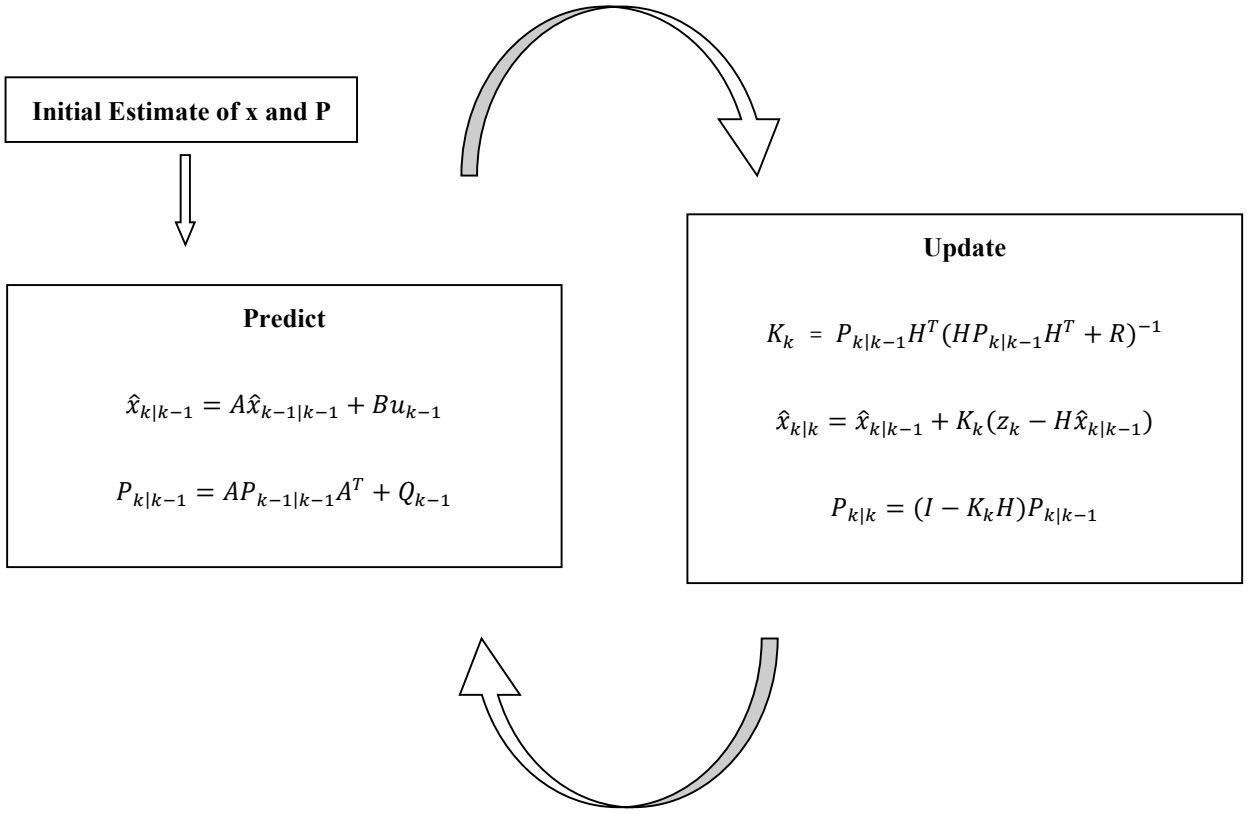


Figure 1. Kalman filter operation diagram.

The adaptive Kalman filter modifies the classic Kalman filter by dynamically adjusting Q and R based on the observed data. This allows the filter to better handle varying noise levels and improve performance. To effectively implement an adaptive Kalman filter for

image denoising, the process involves two main steps: estimating noise statistics and updating the Kalman filter parameters. Firstly, the measurement noise covariance R_k and process noise covariance Q_k are estimated based on the observed noise characteristics in the image. Secondly, these estimated noise statistics are used to dynamically update the Kalman filter parameters at each iteration. The filter is initialized with an initial state. In each iteration, the filter adapts based on the current denoised image, updating R_k and Q_k accordingly. The Kalman filter then denoises the image by predicting and updating pixel values.

3.3. Non-Local Means (NLM) Post-Processing

Following the adaptive Kalman filtering stage, we introduce the non-local means (NLM) algorithm to further enhance the denoising performance. NLM is a powerful technique for image denoising that exploits the redundancy present in natural images. It operates by averaging similar image patches to effectively suppress noise while preserving image details. In our approach, we apply NLM as a post-processing step to refine the denoised image obtained from the adaptive Kalman filtering stage. Specifically, for each pixel in the denoised image, we compute a weighted average of similar patches from the entire image, where the weights are determined based on the similarity between patches. By incorporating NLM into our pipeline, we aim to achieve superior denoising results with enhanced preservation of fine image structures.

Given a noisy image v, the denoised value $u(i)$ at a pixel i is computed as a weighted average of all pixels j in the image. The weight assigned to each pixel j depends on the similarity between the neighborhoods of pixels i and j. The NLM algorithm can be expressed as follows:

$$u(i) = \frac{1}{C(i)} \sum_{j \in \Omega} w(i,j) v(j)$$

where $u(i)$ is the denoised value of the pixel i, Ω is the set of all pixels in the image, and $w(i,j)$ is the weight that measures the similarity between the neighborhoods of pixels i and j. $C(i)$ is a normalization factor ensuring that the weights sum up to 1, and $v(j)$ is the value of the noisy image at pixel j.

The weight $w(i,j)$ is computed as follows:

$$w(i,j) = \exp\left(-\frac{|B(i) - B(j)|^2}{h^2}\right)$$

where h is a filtering parameter that controls the decay of the exponential function and $B(i)$ is the following:

$$B(i) = \frac{1}{|R(i)|} \sum_{q \in R(i)} v(q)$$

where $R(i) \subseteq \Omega$ and is a square region of pixels centered at i and $|R(i)|$ $|\mathrm{R(p)}|$ is the number of pixels in the region R.

3.4. Parameter Selection and Optimization

While the integration of the adaptive Kalman filter and non-local means (NLM) provides a powerful framework for denoising medical images, the effectiveness of NLM heavily relies on the selection of certain parameters. In particular, the denoising performance of NLM is influenced by parameters such as the patch size, search window size, and the similarity threshold.

In this section, we explain the key parameters of the NLM filter, including patch size, search window size, and the similarity threshold, elucidating their respective roles in the denoising process.

Patch Size (W):

The patch size refers to the dimensions of the square or rectangular regions around each pixel considered for comparison. A larger patch size captures more spatial information, enabling the algorithm to better preserve image structures and textures. However, increasing the patch size also increases computational complexity since more patches need to be compared for each pixel.

Search Window Size (S):

The search window size determines the spatial extent within which similar patches are searched for. A larger search window encompasses a wider area for patch comparison, potentially including more diverse image structures and textures. However, a larger search window also increases computational complexity as more patches need to be examined for similarity.

Similarity Threshold (h):

The similarity threshold controls the degree of similarity required for patches to be considered in the averaging process. Lowering the stringency of patch similarity criteria broadens the range of patches included in the denoising process. This results in more aggressive noise reduction but may lead to the loss of fine details and textures due to the incorporation of dissimilar patches. Additionally, this broader inclusion may increase computational overhead as more patches need to be considered for each pixel. Increasing the stringency of patch similarity criteria restricts the inclusion of patches to only those closely resembling the reference patch. This approach preserves more details and textures in the image but might be less effective in reducing noise, especially in the presence of high noise levels. Furthermore, this narrower selection may reduce computational complexity as fewer patches are involved in the denoising operation. Selecting an appropriate similarity threshold is crucial for balancing denoising effectiveness with the preservation of image details and computational efficiency.

3.5. Median Filter Post-Processing

After applying the Kalman filter and non-local means, a further refinement step is employed to enhance the denoised result. This additional post-processing stage involves the application of a median filter.

The median filter is a widely used non-linear filtering technique aimed at reducing noise in digital images while preserving important image features such as edges and textures. It operates by replacing each pixel's value with the median value of the intensities within a defined neighborhood.

The median filter replaces each pixel's value with the median intensity level of its local neighborhood, typically defined by a square or rectangular window. This process effectively removes outliers and reduces noise while preserving edges and fine details in the image. By utilizing the median filter, the residual noise present in the denoised image is further suppressed, leading to an improvement in overall image quality. The effectiveness of the median filter in reducing noise is attributed to its ability to effectively attenuate impulse noise or outliers, which may persist even after the application of the Kalman filter. This is particularly beneficial in scenarios where the denoising algorithm encounters challenges in accurately modeling the noise present in the image.

The choice of the kernel size parameter in the median filter is a critical consideration. It determines the size of the neighborhood over which the median is computed and consequently impacts the trade-off between noise reduction and the preservation of image details. Larger kernel sizes result in more aggressive noise reduction but may also lead to the loss of fine image structures.

Develop hybrid filtering approaches that integrate the adaptive Kalman filter with non-local means and median filtering to effectively address various noise patterns while maintaining computational efficiency. Additionally, combine the outputs of multiple filters using ensemble methods to leverage their strengths, providing more robust denoising across diverse noise types.

3.6. Latin Square Optimization

A Latin square is a mathematical concept used in experimental design and statistics. Latin squares are particularly useful when researchers need to test multiple treatments or conditions while controlling for potential confounding variables. A Latin square is an $n \times n$ grid filled with n different numbers, each appearing exactly once in each row and column. The key characteristic of a Latin square is that no symbol repeats in any row or column. Latin squares have several applications in statistics, especially in experimental design and analysis of variance (ANOVA). They are particularly useful in situations where there are three factors that could influence the outcome of an experiment. By using a Latin square design, researchers can control for these variables and reduce their impact on the results. In other words, Latin squares are a valuable tool in experimental design and statistics, providing a structured approach to controlling for potential sources of variation in an experiment. By using Latin squares, researchers can increase the validity and reliability of their findings, leading to more robust conclusions.

Let L be an $n \times n$ Latin square. We can represent it using a matrix:

$$L = \begin{bmatrix} l_{11} & l_{12} & \cdots & l_{1n} \\ l_{21} & l_{22} & \cdots & l_{2n} \\ \vdots & \vdots & \ddots & \vdots \\ l_{n1} & l_{n2} & \cdots & l_{nn} \end{bmatrix}$$

where l_{ij} represents the element in the i-th row and j-th column of the Latin square.

Now, let us define the properties of a Latin square:

- Each symbol appears exactly once in each row. This can be represented as follows:

$$\forall \mathrm{i} \in \{1,\ 2,\ \ldots,\ \mathrm{n}\},\ \{l_{i1},\ l_{i2},\ \ldots,\ l_{in}\} = \{1,\ 2,\ \ldots,\ \mathrm{n}\}$$

- Each symbol appears exactly once in each column. This can be represented as follows:

$$\forall \mathrm{j} \in \{1,\ 2,\ \ldots,\ \mathrm{n}\},\ \{l_{1j},\ l_{2j},\ \ldots,\ l_{nj}\} = \{1,\ 2,\ \ldots,\ \mathrm{n}\}$$

These conditions together define a Latin square. A Latin square can be constructed given these constraints, and it is a fundamental tool in experimental design.

Latin square designs are widely used in experimental research to control for multiple sources of variation and assess the effects of different factors on the outcome of interest. One key aspect of analyzing the data obtained from Latin square designs is the utilization of statistical models to understand the relationships between various factors and the observed responses.

In this regard, the formula $y_{ijk} = \mu + \alpha_i + \tau_j + \beta_k + \varepsilon_{ijk}$ plays a crucial role. This formula represents a linear model commonly used in the analysis of variance (ANOVA) for Latin square designs. It decomposes the observed response variable y_{ijk} into several components, each representing a different source of variation. Now, let us analyze the elements of this equation:

y_{ijk}: This represents the observed response or outcome variable for the i-th row, j-th column, and k-th treatment condition in the Latin square design.

μ: This is the overall mean of all observations in the Latin square, serving as a baseline reference point.

α_i: This term represents the effect of the i-th row in the Latin square, capturing the systematic variation attributable to differences between rows.

τ_j: Similarly, this term represents the effect of the j-th column in the Latin square, accounting for systematic variation between columns.

β_k: This term represents the effect of the k-th treatment condition, capturing systematic variation attributable to differences between treatments.

ε_{ijk}: Finally, this term represents the random error or residual, capturing the unexplained variability in the observed response variable that cannot be accounted for by the row, column, or treatment effects.

In our study, we utilized the formula $y_{ijk} = \mu + \alpha_i + \tau_j + \beta_k + \varepsilon_{ijk}$ as a framework to optimize the parameters for the non-local means algorithm. Specifically, we mapped the components of the formula to the parameters of the non-local means algorithm, which include α_i as the parameter h, τ_j as the parameter TemplateWindowSize, and β_k as the parameter SearchWindowSize.

To optimize these parameters, we conducted experiments using two different quality metrics: the peak signal-to-noise ratio (PSNR) and mean squared error (MSE). When optimizing for PSNR, we aimed to maximize the PSNR value, which corresponds to maximizing image quality and minimizing noise distortion. Conversely, when optimizing for MSE, we aimed to minimize the MSE value, indicating minimal discrepancy between the denoised image and the ground truth.

Our experimental approach involved running the non-local means algorithm with varying parameter values and evaluating the resulting PSNR and MSE values. For PSNR optimization, we identified the parameter values that yielded the highest PSNR, indicating the most effective noise reduction while preserving image quality. Conversely, for MSE optimization, we sought the parameter values that minimized the MSE, indicating the closest match between the denoised image and the ground truth.

By leveraging the framework provided by the ANOVA model and carefully selecting parameter values based on PSNR and MSE optimization, we were able to customize the non-local means algorithm to achieve optimal noise reduction performance while preserving image quality in our experimental setup.

In our study, we employed Latin square designs to efficiently determine the optimal parameters for the non-local means algorithm while minimizing the complexity of experiments. Latin square designs enable systematic experimentation by controlling for multiple sources of variation, thereby allowing us to explore the effects of different parameter combinations in a structured and efficient manner. Without the use of Latin square designs, the process of finding the best parameters for the non-local means algorithm would entail exhaustive experimentation, involving n^3 complexity. This arises from the need to evaluate all possible combinations of parameters across the three dimensions of h, TemplateWindowSize, and SearchWindowSize, each ranging from 1 to n. This exhaustive search approach becomes increasingly impractical as the number of parameters and their ranges of values grow, leading to significant computational overhead and time requirements. By leveraging Latin square designs, we were able to substantially reduce the degree of complexity to n^2. This reduction in complexity stems from the structured arrangement of parameter combinations within the Latin square design, which ensures that each parameter is tested at n levels while controlling for the effects of other parameters. As a result, Latin square designs enable a more efficient exploration of parameter space, allowing us to identify optimal parameter settings with fewer experiments and computational resources.

Latin square optimization is particularly advantageous due to its efficiency and robustness, which are crucial attributes in parameter selection for non-local means. It ensures a comprehensive and balanced exploration of the parameter space with fewer evaluations. The efficiency gained through the use of Latin square designs is particularly advantageous in the context of parameter optimization for image processing algorithms such as non-local means. By minimizing the complexity of experiments, Latin square designs facilitate rapid experimentation and parameter tuning, enabling researchers to efficiently identify parameter settings that optimize algorithm performance while mitigating computational overhead. The algorithm for selecting optimized variables using a Latin square is presented in Algorithm 1.

Algorithm 1: Selection of Optimized Variables Using a Latin Square.

1: Input: Parameters = {W,S,h} and n levels for parameters
W = $\{W_1, W_2, \ldots, W_n\}$, S = $\{S_1, S_2, \ldots, S_n\}$, and h = $\{h_1, h_2, \ldots, h_n\}$
2: Output: Optimal levels for parameters
3: Initialize a Latin Square with n × n matrix
Assign the parameters such that each parameter appears exactly once in each row and each column
4: **for** i in (0..n) **do**
5: **for** j in (0..n) **do**
6: table[i][j] = f (W_i, S_j)
7: **for** k in (0..n) **do**
derive $y_{ijk} = \mu + \alpha_i + \tau_j + \beta_k + \varepsilon_{ijk}$
8: **end for**
9: **end for**
10: **end for**
11: solve the equations
12: **if** y_{ijk} == MSE **then**
13: Minimize the Objective Function
14: **else if** y_{ijk} == PSNR **then**
15: Maximize the Objective Function
16: **else**
17: Invalid choice
18: **end if**
19: determine the optimal parameters
20: **return** optimal parameters

4. Experimental Results

In this section, we present the experimental results, which are divided into two subsections. Firstly, in Section 3.1, we discuss the findings from the Latin Square analysis. Subsequently, in Section 3.2, we delve into the evaluation results of our proposed method.

4.1. Analysis Results Latin Square

In this subsection, we present the results of the Latin square analysis conducted to determine the optimal parameters for the non-local means denoising method. We used a 5 × 5 Latin square matrix and in this matrix, each row represents a different level of the first parameter, each column represents a different level of the second parameter, and each entry represents the different value of the third parameters. We systematically varied these parameters across different values to comprehensively explore their impact on denoising performance. The parameters under consideration include h as well as the TemplateWindowSize and SearchWindowSize. The values assigned to each parameter combination are summarized in Table 1.

$$\text{Parameter Variation Matrix} = \begin{bmatrix} 1 & 2 & 3 & 4 & 5 \\ 2 & 1 & 4 & 5 & 3 \\ 3 & 5 & 1 & 2 & 4 \\ 4 & 3 & 5 & 1 & 2 \\ 5 & 4 & 2 & 3 & 1 \end{bmatrix}$$

Table 1. Parameters for non-local means denoising method in Latin square analysis.

h	TemplateWindowSize	SearchWindowSize
5	3	8
7	5	10
9	7	15
10	9	20
12	12	25

To solve the equation $y_{ijk} = \mu + \alpha_i + \tau_j + \beta_k + \varepsilon_{ijk}$ and find the values for μ, α, τ, and β, we can represent the values of PSNR and MSE in matrices. We have three parameters, each with five possible states. Therefore, we have five values each for α, τ, and β. The dependent variable can either be PSNR or MSE. Note that if the dependent variable is PSNR, the objective function should be maximized, while if it is MSE, the objective function should be minimized. The selection of the independent variable is based on the parameter variation matrix. The index of α corresponds to the row number, the index of τ corresponds to the column number, and the index of β corresponds to the element number within the parameter variation matrix. Let us denote PSNR as $PSNR_{ijk}$ and MSE as MSE_{ijk}. The analysis is centered on the first image (Image I), which has been subjected to Gaussian noise. The Gaussian noise parameters are configured with a mean value set to the default of 0 and a standard deviation set to 25. Then, we can represent the values of PSNR and MSE in matrices as follows:

$$PSNR = \begin{bmatrix} 33.020 & 33.007 & 33.007 & 33.007 & 33.007 \\ 33.168 & 33.048 & 33.068 & 33.057 & 33.021 \\ 33.453 & 33.413 & 33.192 & 33.186 & 33.165 \\ 33.509 & 33.449 & 33.369 & 33.3 & 33.291 \\ 33.412 & 33.32 & 33.446 & 33.269 & 33.465 \end{bmatrix}$$

$$MSE = \begin{bmatrix} 32.437 & 32.532 & 32.535 & 32.535 & 32.535 \\ 31.345 & 32.229 & 32.077 & 32.161 & 32.432 \\ 29.356 & 29.633 & 31.180 & 31.223 & 31.370 \\ 28.978 & 29.383 & 29.933 & 30.407 & 30.471 \\ 29.639 & 30.274 & 29.408 & 30.629 & 29.274 \end{bmatrix}$$

We solved the equations and obtained the values for μ, α, τ, and β. The results are depicted in Table 2.

Table 2. Optimal parameter values.

Parameters	PSNR	MSE
μ	20.766225	19.3494
α_1	3.936885	5.42564
α_2	3.999685	4.95964
α_3	4.209085	3.46324
α_4	4.310885	2.74524
α_5	4.309685	2.75564
τ_1	4.239685	3.26184
τ_2	4.174685	3.72104
τ_3	4.143685	3.93744
τ_4	4.091085	4.30184
τ_5	4.117085	4.12724
β_1	4.132285	4.01624
β_2	4.146885	3.90664
β_3	4.167085	3.77784
β_4	4.141085	3.95764
β_5	4.178885	3.69104

To determine the optimal parameters for denoising, we formulated an objective function tailored to the desired performance metric. For PSNR optimization, the objective function aimed to maximize PSNR, leading to the selection of parameter values that yield

the highest PSNR values. Conversely, for MSE optimization, the objective function aimed to minimize MSE, resulting in the selection of parameter values that produce the lowest MSE values. Remarkably, the optimization objectives for both PSNR and MSE converge to the same parameter values. As illustrated in Table 2, the optimal values for α, τ, and β are consistent across both PSNR and MSE metrics, with α_4, τ_1, and β_5 being selected. Consequently, h = 10, TemplateWindowSize = 3, and SearchWindowSize = 25 emerge as the best parameter choices, demonstrating their effectiveness in enhancing denoising performance across both PSNR and MSE criteria.

4.2. Proposed Method Evaluation Results

The experimental evaluation utilized the Breast Ultrasound Images Dataset sourced [29], providing a robust foundation for assessing the efficacy of the proposed methodologies. The Breast Ultrasound Images Dataset utilized in this study comprises a diverse collection of imaging data obtained from female participants aged between 25 and 75 years old during the year 2018. The dataset includes information from 600 women and consists of 780 ultrasound images, each stored in PNG format with an average size of 500 $\times$ 500 pixels. These images are categorized into three distinct classes: normal, benign, and malignant, providing valuable insights into breast health and pathology. Specifically, the dataset comprises 487 benign, 210 malignant, and 133 normal images, allowing for comprehensive analysis and exploration of breast tissue characteristics across varying clinical conditions [29].

Employing an adaptive Kalman filter augmented with non-local means and median as post-processing techniques facilitated significant noise reduction in medical images. To streamline the experimental process and ensure a thorough analysis, a Latin square design was employed, effectively minimizing experimental complexity.

Two prevalent types of noise, Gaussian and Poisson, were intentionally introduced into the medical images to simulate real-world conditions and comprehensively evaluate the robustness of the proposed denoising approach. Gaussian noise was characterized by its additive nature and normally distributed intensity variations. Meanwhile, Poisson noise, arising from the statistical fluctuations in photon counts during image acquisition, represented another common source of noise in medical imaging.

To ensure the optimal performance of the proposed denoising methodology, a systematic parameter optimization process was conducted utilizing a Latin square design. This experimental design methodology enabled the efficient exploration of multiple parameter combinations while minimizing the influence of confounding variables, thus enhancing the reliability and validity of the experimental results. Specifically, the parameters of the non-local means algorithm, a key component of the denoising approach, were systematically varied and evaluated across different configurations. The Latin square design facilitated the generation of a balanced set of parameter combinations, ensuring an equitable representation of each parameter value across different experimental runs. By systematically varying parameters such as patch size, search window size, and the similarity threshold, the Latin square design allowed for a comprehensive exploration of the parameter space while controlling for potential biases and confounding factors.

Quantitative assessments were conducted using standard image quality metrics, including the Peak Signal-to-Noise Ratio (PSNR), Mean Squared Error (MSE), and Structural Similarity Index (SSIM). These metrics served as objective measures to evaluate the performance of the proposed approach in comparison to existing methods. Let us provide a more comprehensive description of those parameters.

- Peak Signal-to-Noise Ratio (PSNR):

PSNR measures the quality of a reconstructed or denoised image by comparing it to the original image. It measures the ratio between the maximum possible power of a signal and the power of corrupting noise that affects the fidelity of its representation. It is

commonly used to evaluate the quality of denoised or compressed images. Higher PSNR values indicate better image quality, with lower levels of distortion or noise.

$$PSNR = 10\, log_{10}\left(\frac{MAX^2}{MSE}\right)$$

where MAX is the maximum possible pixel value of the image (typically 255 for 8-bit grayscale images) and MSE is the Mean Squared Error.

- Mean Squared Error (MSE):

MSE measures the average squared difference between the original image and the denoised image, with higher MSE values indicating greater distortion or noise.

$$MSE = \frac{1}{N}\sum_{i=1}^{N}(I(i) - K(i))^2$$

where N is the total number of pixels in the image, $I(i)$ is the intensity of the ith pixel in the original image, and $K(i)$ is the intensity of the ith pixel in the processed (denoised) image.

- Structural Similarity Index (SSIM):

SSIM assesses the similarity between two images by comparing local patterns of pixel intensities, considering luminance, contrast, and structure. It aims to capture perceived differences in image quality, aligning more closely with human visual perception than traditional pixel-wise metrics like PSNR and MSE. Higher SSIM values indicate greater similarity between the original and processed images. The justification for using SSIM lies in its ability to account for perceived differences in image quality, rather than focusing solely on pixel-wise differences. SSIM considers both local and global image features, making it more robust to changes in image content and illumination.

$$SSIM(x, y) = \frac{(2\mu_x\mu_y + C_1)(2\sigma_{xy} + C_2)}{\left(\mu_x^2 + \mu_y^2 + C_1\right)\left(\sigma_x^2 + \sigma_y^2 + C_2\right)}$$

where x and y are the compared image patches, μ is the mean, σ_{xy} is the covariance of x and y, σ is the variance, and C is the constant to stabilize the division with a weak denominator.

To assess the effectiveness of the proposed denoising methodology, we compared the proposed method with the median filter, non-local means (NLM) filter, Kalman filter, and the Kalman filter followed by a non-local means filter as a post-processing step. In Tables 3 and 5, we present the results of this comparison under different noise conditions. In Table 3, we compared the proposed method with various denoising techniques when the image is corrupted with Gaussian noise. The Gaussian noise parameters are configured with a mean value set to the default of 0 and a standard deviation set to 25. These parameters are pivotal in shaping the noise characteristics within the image, influencing its overall quality and appearance. The performance metrics including PSNR, MSE, and SSIM are reported for both methods, demonstrating the superiority of our proposed approach in terms of image quality enhancement.

The improvement of the proposed method compared to various denoising approaches under Gaussian noise is shown in Table 4. On average, the proposed method achieves a notable improvement in PSNR values, indicating enhanced signal fidelity and reduced noise interference across the dataset. Additionally, there is a substantial decrease in MSE values, signifying improved accuracy in image reconstruction and reduced distortion in the denoised images. This reduction highlights the effectiveness of the proposed methodology in mitigating noise artifacts. Furthermore, SSIM scores demonstrate remarkable enhancement, emphasizing the preservation of important structural details and perceptual quality in the denoised images, which aligns more closely with human visual perception.

Table 3. Comparison of denoising approaches with the proposed method under Gaussian noise.

Gaussian Noise		Image I	Image II	Image III	Image IV	Image V	Image VI	Image VII	Image VIII	Image IX	Image X
Median	PSNR	27.64	27.32	27.54	27.43	27.70	27.73	27.75	27.66	28.01	27.86
	MSE	111.97	120.46	114.70	117.44	110.47	109.72	109.23	111.50	102.94	106.37
	SSIM	0.599	0.657	0.638	0.633	0.635	0.609	0.637	0.567	0.591	0.607
NLM	PSNR	24.17	23.49	23.21	24.96	25.95	25.18	25.28	23.23	24.07	25.22
	MSE	248.74	291.18	310.72	207.53	165.06	197.35	192.87	308.95	254.70	195.67
	SSIM	0.498	0.521	0.464	0.576	0.632	0.571	0.589	0.399	0.459	0.547
Kalman	PSNR	29.07	29.01	29.13	29.02	29.03	29.07	29.10	29.15	29.25	29.19
	MSE	80.49	81.51	79.41	81.42	81.20	80.52	79.83	78.94	77.16	78.19
	SSIM	0.413	0.498	0.478	0.458	0.431	0.411	0.434	0.403	0.387	0.402
Kalman and NLM	PSNR	27.00	26.01	26.77	26.02	26.32	27.06	26.29	28.10	27.56	26.99
	MSE	129.61	163.11	136.93	162.71	151.66	127.97	152.89	100.65	114.08	130.10
	SSIM	0.634	0.656	0691	0.594	0.584	0.611	0.585	0.690	0.610	0.596
Proposed Method	PSNR	33.52	32.22	32.66	32.36	33.31	33.45	32.65	33.30	33.16	32.93
	MSE	28.88	38.93	35.24	37.73	30.30	29.36	35.26	30.40	31.34	33.04
	SSIM	0.842	0.821	0.834	0.816	0.853	0.843	0.814	0.811	0.807	0.807

Table 4. Comparison of improvement between proposed method and various denoising approaches under Gaussian noise.

Gaussian Noise	Median			NLM			Kalman			Kalman and NLM		
	PSNR	MSE	SSIM	PSNR	MSE	SSIM	PSNR	MSE	SSIM	PSNR	MSE	SSIM
Improvement %	19.12	70.38	33.82	34.82	85.49	59.54	13.24	58.63	92.24	22.95	75.58	20.38

To evaluate the effectiveness of the proposed denoising method, we present the visual results obtained from processing a noisy image using both the Kalman filter and our proposed approach. The original images utilized in this research are depicted in Figure 2.

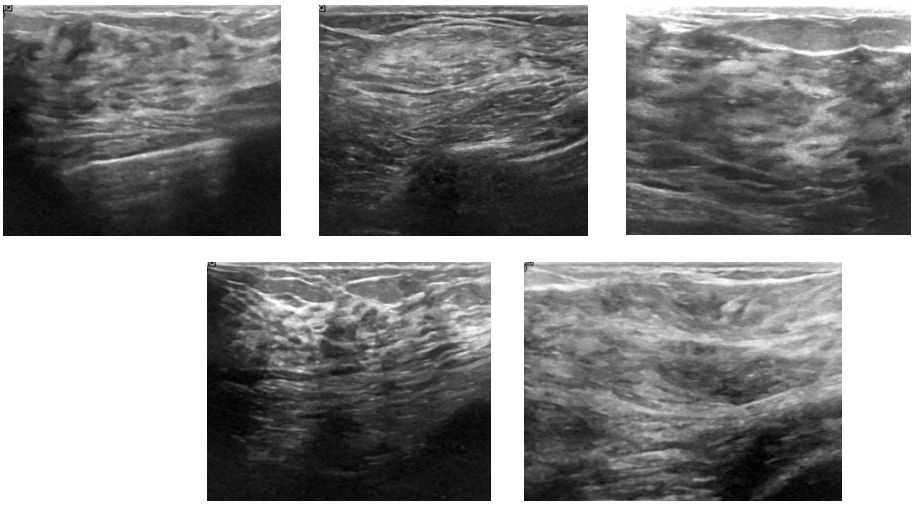


Figure 2. Original images.

The noisy image, corrupted with Gaussian noise, is depicted in Figure 3, illustrating the significant degradation caused by the noise. After applying the denoising techniques, we observe noticeable improvements in image quality. The denoised image obtained with the Kalman filter demonstrates reduced noise levels, albeit with residual artifacts. Conversely, our proposed approach not only suppresses noise effectively but also preserves finer details and textures, resulting in a visually pleasing image with enhanced clarity and fidelity. The visual comparison provides compelling evidence of the superior performance of our proposed method in restoring images corrupted by Gaussian noise.

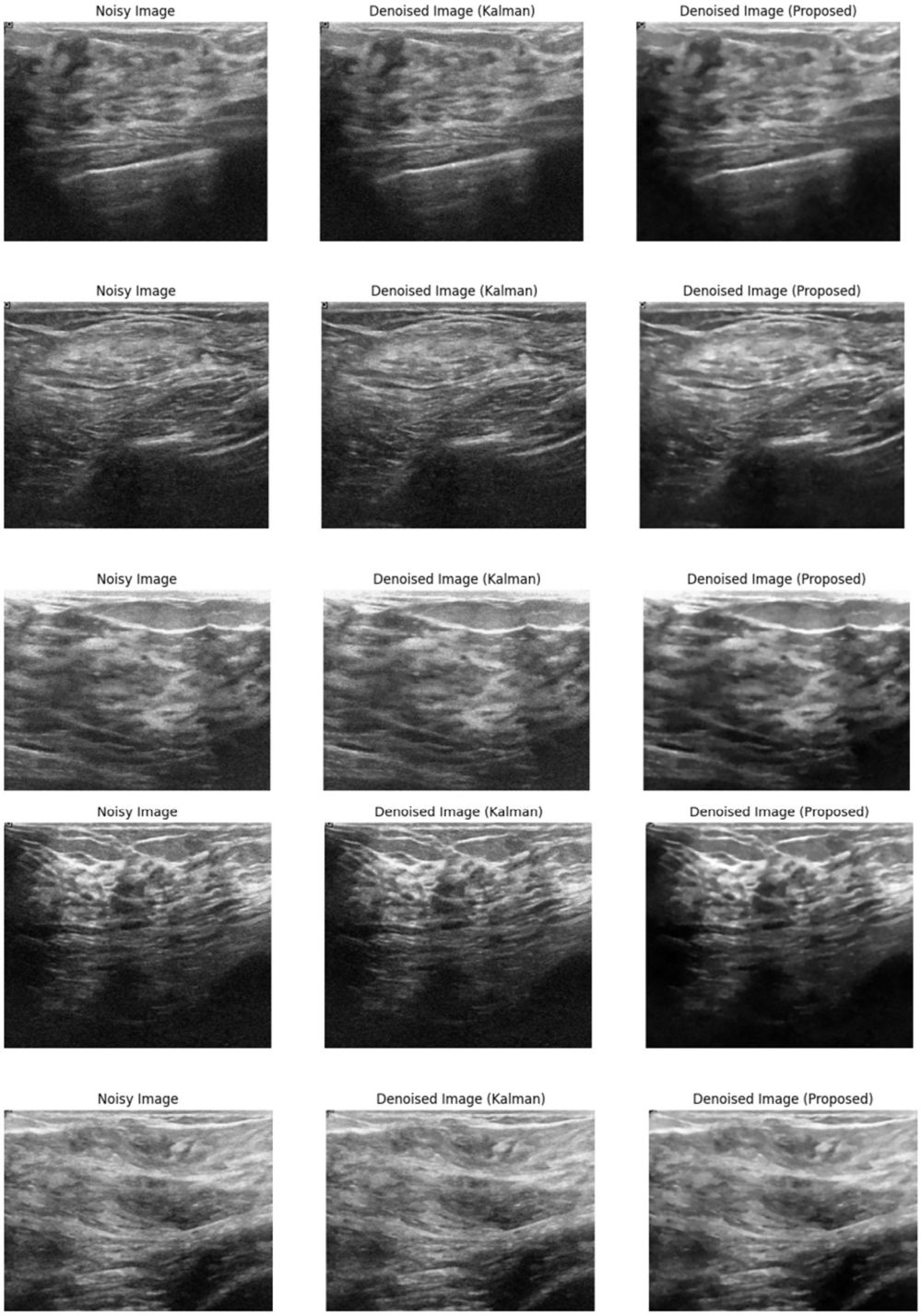


Figure 3. Visual comparison of noisy image corrupted with Gaussian noise, denoised image with Kalman filter, and denoised image with proposed approach.

The zoomed-in section of the noisy image under Gaussian noise is depicted in Figure 4. The denoised image using the Kalman filter is shown on the left side, while the denoised image using the proposed method is shown on the right side.

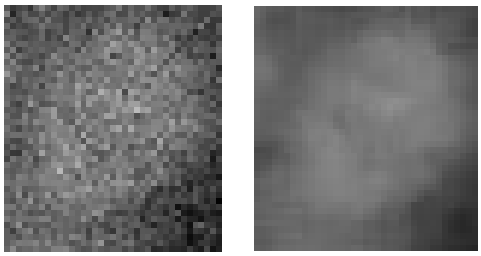


Figure 4. Zoomed-in comparison of denoised images using Kalman filter (**Left**) and proposed method (**Right**) under Gaussian noise.

Table 5 presents a comparative analysis of the proposed method with the median filter, non-local means (NLM) filter, Kalman filter, and the Kalman filter followed by the non-local means filter as a post-processing step under Poisson noise conditions. The parameters of the Poisson noise are determined by scaling the normalized pixel values of the image, which are used to establish the mean for the Poisson distribution. Similar to the Gaussian noise scenario, the evaluation metrics highlight the effectiveness of our methodology in mitigating noise and preserving image quality. The comparative analysis reveals notable improvements in various image quality metrics achieved by the proposed denoising methodology.

Table 5. Comparison of denoising approaches with the proposed method under Poisson noise.

Poisson Noise		Image I	Image II	Image III	Image IV	Image V	Image VI	Image VII	Image VIII	Image IX	Image X
Median	PSNR	32.92	32.31	32.82	31.74	32.12	32.16	32.34	32.91	33.50	32.58
	MSE	33.21	38.16	33.95	43.54	39.89	39.58	37.97	33.28	29.02	35.87
	SSIM	0.859	0.880	0.892	0.835	0.837	0.833	0.851	0.856	0.862	0.849
NLM	PSNR	32.70	31.98	32.48	30.88	32.11	32.03	32.21	32.25	33.53	32.69
	MSE	34.96	41.20	36.70	53.10	39.97	40.74	39.08	38.77	28.86	34.98
	SSIM	0.851	0.857	0.880	0.808	0.837	0.826	0.838	0.836	0.860	0.841
Kalman	PSNR	31.72	31.66	32.24	30.93	30.87	31.09	31.22	32.35	32.22	31.61
	MSE	43.69	44.35	38.77	52.40	53.17	50.53	49.00	37.85	38.98	44.81
	SSIM	0.762	0.817	0.832	0.740	0.709	0.704	0.744	0.785	0.768	0.744
Kalman and NLM	PSNR	34.14	33.19	33.12	32.88	34.16	33.87	33.85	33.41	34.26	34.15
	MSE	25.04	31.16	31.68	33.51	24.98	26.65	26.79	29.63	24.39	25.03
	SSIM	0.867	0.871	0.869	0.862	0.882	0.861	0.876	0.838	0.851	0.861
Proposed Method	PSNR	34.92	33.35	33.96	33.48	34.96	34.96	34.53	34.32	35.55	35.09
	MSE	20.93	29.99	26.07	29.13	20.72	20.73	22.89	24.00	18.08	20.12
	SSIM	0.889	0.870	0.887	0.857	0.902	0.894	0.891	0.853	0.891	0.888

The improvement of the proposed method compared to various denoising approaches under Poisson noise is shown in Table 6.

Table 6. Comparison of improvement between proposed method and various denoising approaches under Poisson noise.

Poisson Noise	Median			NLM			Kalman			Kalman and NLM		
	PSNR	MSE	SSIM	PSNR	MSE	SSIM	PSNR	MSE	SSIM	PSNR	MSE	SSIM
Improvement %	6.06	35.95	3.18	6.90	39.80	4.63	9.27	48.02	16.35	2.39	16.92	2.13

To further evaluate the robustness and efficacy of our proposed denoising method, we present the visual results obtained from processing images corrupted with Poisson noise. Figure 5 illustrates the degradation caused by Poisson noise. Despite the inherent complexities associated with Poisson noise, our proposed denoising approach effectively mitigates its adverse effects, resulting in denoised images that exhibit improved clarity and fidelity. Comparative analysis with denoised images obtained using traditional denoising techniques, such as the Kalman filter, highlights the superior performance of our proposed method in restoring images affected by Poisson noise. These visual results underscore the

effectiveness of our approach in addressing the diverse noise types encountered in practical imaging scenarios.

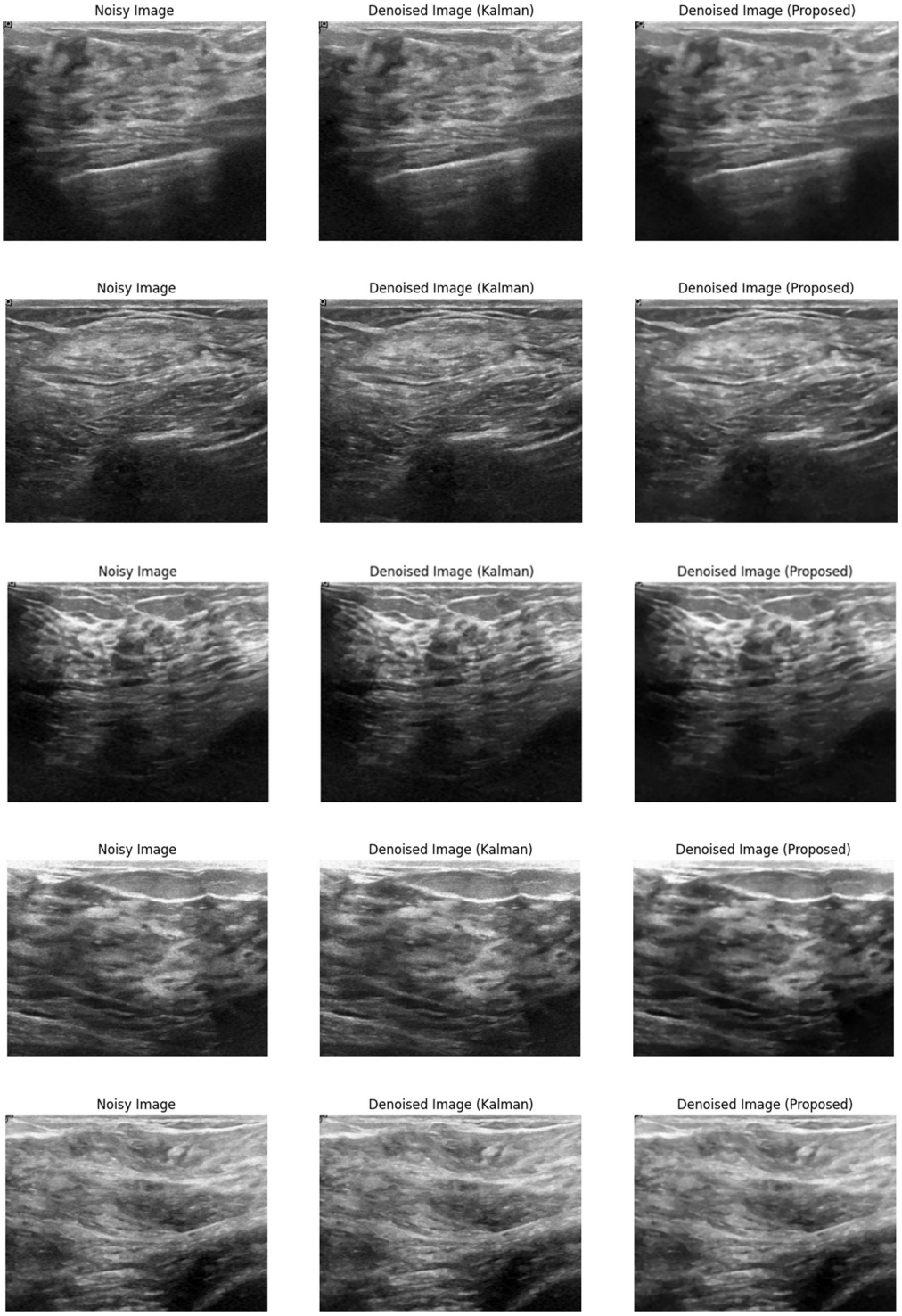


Figure 5. Visual comparison of noisy image corrupted with Poisson noise, denoised image with Kalman filter, and denoised image with proposed approach.

The zoomed-in section of the noisy image under Poisson noise is depicted in Figure 6. The denoised image using the Kalman filter is shown on the left side, while the denoised image using the proposed method is shown on the right side.

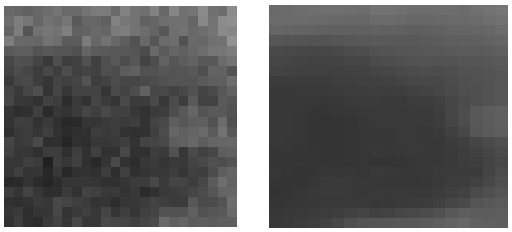


Figure 6. Zoomed-in comparison of denoised images using Kalman filter (**Left**) and proposed method (**Right**) under Poisson noise.

In Table 7, the percentage of robustness of the proposed method, compared to the Kalman filter, in the presence of Gaussian and Poisson noise is illustrated. We present the results of a robustness analysis conducted to evaluate the resilience of the proposed denoising method under increased noise levels. The parameters for Gaussian and Poisson noise are detailed in Section 4.2. By systematically augmenting the noise on the original image, we measured the resulting PSNR and MSE values using the proposed method and compared them with those obtained using a Kalman filter. The robustness of our system is demonstrated by identifying the maximum level of noise augmentation at which the PSNR and MSE values remain consistent with those achieved using the Kalman filter. This critical threshold represents the point at which the proposed method effectively mitigates the increased noise, maintaining comparable image quality metrics to the baseline approach. By determining the maximum allowable noise augmentation while preserving consistent PSNR and MSE values, we provide valuable insights into the robustness and reliability of the proposed denoising methodology in real-world scenarios. This analysis underscores the resilience of our system and its capacity to maintain high-quality denoised images across a range of noise levels, enhancing its practical utility in medical imaging applications.

Table 7. Robustness analysis of the proposed method compared to Kalman filter.

Robustness (%)	Gaussian	Poisson
Image I	43.37	36.69
Image II	43.96	29.49
Image III	38.88	27.88
Image IV	47.01	35.80
Image V	47.28	38.98

The standard deviation of the initial noise is 25, which provided a baseline level of image degradation. To further investigate the impact on image quality, we increased the standard deviation of the noise to 91, resulting in a significant decrease in PSNR, indicating higher noise level. For Poisson noise, which is inherently dependent on the image intensity, the deviation range caused both noticeable darkening and brightening in different regions of the image and we observed a significant decline in the PSNR.

We developed an algorithm to systematically evaluate its performance under varying noise levels. Algorithm 2 illustrates the procedure for determining the maximum noise level at which our method maintains consistent image quality metrics, such as PSNR and MSE. This analysis provides valuable insights into the resilience of our denoising approach in real-world scenarios.

Algorithm 2: Robustness Analysis.

```
Input:
        - OriginalImage: the original image
        - MaxNoiseLevel: the maximum noise level to be tested
        - ProposedMethod: function to apply the proposed denoising method
        - DesiredOutputPSNR: the desired PSNR value for the denoised image
        - DesiredOutputMSE: the desired MSE value for the denoised image

    Output:
        - MaxNoiseLevel: the maximum noise level at which PSNR and MSE
        remain consistent

    Initialize NoiseLevel to image noise level

    For NoiseLevel from the image noise level to MaxNoiseLevel:
        Add noise to OriginalImage with NoiseLevel
        Calculate PSNR of the noisy image

Denoise the noisy image using ProposedMethod
Calculate PSNR and MSE of the denoised image
        If PSNR of noisy image > DesiredOutputPSNR or MSE of noisy
        image < DesiredOutputMSE:
        Increment NoiseLevel

    Return MaxNoiseLevel
```

5. Conclusions

This paper presents a pioneering hybrid approach for medical image denoising, addressing the crucial need for preserving image details while effectively reducing noise. By introducing an adaptive Kalman filter that dynamically adjusts its parameters based on the input image's noise characteristics, we achieve improved accuracy in estimating the underlying true state of the system. The subsequent post-processing steps involving non-local means (NLM) and median filtering further refine the denoised image, enhancing noise reduction while preserving essential image features. The innovative use of Latin square optimization enables efficient parameter selection for NLM, mitigating the complexity of experiments without compromising denoising performance. The experimental results underscore the effectiveness of our approach, showcasing substantial enhancements over conventional methods. This work not only advances the state-of-the-art in medical image denoising but also offers a practical solution for optimizing parameter selection in NLM, thereby fostering their wider adoption in medical imaging applications.

Author Contributions: Conceptualization, M.T. and B.V.; methodology, M.T. and B.V.; software, M.T.; validation, M.T. and B.V.; formal analysis, M.T. and B.V.; investigation, M.T. and B.V.; resources, M.T.; data curation, M.T.; writing—original draft preparation, M.T.; writing—review and editing, M.T. and B.V.; supervision, B.V. and M.T. All authors have read and agreed to the published version of the manuscript.

Funding: This research received no external funding.

Data Availability Statement: The data can be shared up on request.

Conflicts of Interest: The authors declare no conflict of interest.

References

1. Chang, S.G.; Yu, B.; Vetterli, M. Adaptive wavelet thresholding for image denoising and compression. *IEEE Trans. Image Process.* **2000**, *9*, 1532–1546. [CrossRef] [PubMed]
2. Starck, J.L.; Candès, E.J.; Donoho, D.L. The curvelet transform for image denoising. *IEEE Trans. Image Process.* **2002**, *11*, 670–684. [CrossRef] [PubMed]

3. Elad, M.; Aharon, M. Image denoising via sparse and redundant representations over learned dictionaries. *IEEE Trans. Image Process.* **2006**, *15*, 3736–3745. [CrossRef] [PubMed]
4. Dong, W.; Zhang, L.; Shi, G.; Li, X. Nonlocally centralized sparse representation for image restoration. *IEEE Trans. Image Process.* **2012**, *22*, 1620–1630. [CrossRef] [PubMed]
5. Zhou, M.; Chen, H.; Paisley, J.; Ren, L.; Li, L.; Xing, Z.; Dunson, D.; Sapiro, G.; Carin, L. Nonparametric Bayesian dictionary learning for analysis of noisy and incomplete images. *IEEE Trans. Image Process.* **2011**, *21*, 130–144. [CrossRef] [PubMed]
6. Portilla, J.; Strela, V.; Wainwright, M.J.; Simoncelli, E.P. Image denoising using scale mixtures of Gaussians in the wavelet domain. *IEEE Trans. Image Process.* **2003**, *12*, 1338–1351. [CrossRef] [PubMed]
7. Luo, E.; Chan, S.H.; Nguyen, T.Q. Adaptive image denoising by targeted databases. *IEEE Trans. Image Process.* **2015**, *24*, 2167–2181. [CrossRef] [PubMed]
8. Zhang, K.; Zuo, W.; Chen, Y.; Meng, D.; Zhang, L. Beyond a gaussian denoiser: Residual learning of deep cnn for image denoising. *IEEE Trans. Image Process.* **2017**, *26*, 3142–3155. [CrossRef] [PubMed]
9. Rabie, T. Robust estimation approach for blind denoising. *IEEE Trans. Image Process.* **2005**, *14*, 1755–1765. [CrossRef]
10. Liu, C.; Szeliski, R.; Kang, S.B.; Zitnick, C.L.; Freeman, W.T. Automatic estimation and removal of noise from a single image. *IEEE Trans. Pattern Anal. Mach. Intell.* **2007**, *30*, 299–314. [CrossRef]
11. Lebrun, M.; Colom, M.; Morel, J.M. Multiscale image blind denoising. *IEEE Trans. Image Process.* **2015**, *24*, 3149–3161. [CrossRef]
12. Zhu, F.; Chen, G.; Hao, J.; Heng, P.A. Blind image denoising via dependent Dirichlet process tree. *IEEE Trans. Pattern Anal. Mach. Intell.* **2016**, *39*, 1518–1531. [CrossRef] [PubMed]
13. Xu, J.; Zhang, L.; Zhang, D. External prior guided internal prior learning for real-world noisy image denoising. *IEEE Trans. Image Process.* **2018**, *27*, 2996–3010. [CrossRef] [PubMed]
14. Khodarahmi, M.; Maihami, V. A review on Kalman filter models. *Arch. Comput. Methods Eng.* **2023**, *30*, 727–747. [CrossRef]
15. Ma, R.; Hu, H.; Xing, S.; Li, Z. Efficient and fast real-world noisy image denoising by combining pyramid neural network and two-pathway unscented Kalman filter. *IEEE Trans. Image Process.* **2020**, *29*, 3927–3940. [CrossRef]
16. Conte, F.; Germani, A.; Iannello, G. A kalman filter approach for denoising and deblurring 3-d microscopy images. *IEEE Trans. Image Process.* **2013**, *22*, 5306–5321. [CrossRef] [PubMed]
17. Roonizi, A.K.; Selesnick, I.W. A Kalman filter framework for simultaneous LTI filtering and total variation denoising. *IEEE Trans. Signal Process.* **2022**, *70*, 4543–4554. [CrossRef]
18. Yang, L.; Parton, R.; Ball, G.; Qiu, Z.; Greenaway, A.H.; Davis, I.; Lu, W. An adaptive non-local means filter for denoising live-cell images and improving particle detection. *J. Struct. Biol.* **2010**, *172*, 233–243. [CrossRef]
19. Zhang, X. Two-step non-local means method for image denoising. *Multidimens. Syst. Signal Process.* **2022**, *33*, 341–366. [CrossRef]
20. Arabi, H.; Zaidi, H. Non-local mean denoising using multiple PET reconstructions. *Ann. Nucl. Med.* **2021**, *35*, 176–186. [CrossRef]
21. Bal, A.; Banerjee, M.; Chaki, R.; Sharma, P. An efficient method for PET image denoising by combining multi-scale transform and non-local means. *Multimed. Tools Appl.* **2020**, *79*, 29087–29120. [CrossRef]
22. Jiang, J.; Yang, K.; Yang, J.; Yang, Z.X.; Chen, Y.; Luo, L. A new nonlocal means based framework for mixed noise removal. *Neurocomputing* **2021**, *431*, 57–68. [CrossRef]
23. Pan, J.; Yang, X.; Cai, H.; Mu, B. Image noise smoothing using a modified Kalman filter. *Neurocomputing* **2016**, *173*, 1625–1629. [CrossRef]
24. Pfleger, S.G.; Plentz, P.D.; Rocha, R.C.; Pereira, A.D.; Castro, M. Real-time video denoising on multicores and gpus with kalman-based and bilateral filters fusion. *J. Real-Time Image Process.* **2019**, *16*, 1629–1642. [CrossRef]
25. Wang, X.; Su, Y.; Xu, M.; Zhang, H.; Zhang, Y. A new image encryption algorithm based on Latin square matrix. *Nonlinear Dyn.* **2022**, *107*, 1277–1293. [CrossRef]
26. Hua, Z.; Zhu, Z.; Chen, Y.; Li, Y. Color image encryption using orthogonal Latin squares and a new 2D chaotic system. *Nonlinear Dyn.* **2021**, *104*, 4505–4522. [CrossRef]
27. Zhou, J.; Zhou, N.R.; Gong, L.H. Fast color image encryption scheme based on 3D orthogonal Latin squares and matching matrix. *Opt. Laser Technol.* **2020**, *131*, 106437. [CrossRef]
28. Reid, I.; Term, H. *Estimation ii*; Lecture Note; University of Oxford: Oxford, UK, 2001.
29. Al-Dhabyani, W.; Gomaa, M.; Khaled, H.; Fahmy, A. Dataset of breast ultrasound images. *Data Brief* **2020**, *28*, 104863. [CrossRef]

Disclaimer/Publisher's Note: The statements, opinions and data contained in all publications are solely those of the individual author(s) and contributor(s) and not of MDPI and/or the editor(s). MDPI and/or the editor(s) disclaim responsibility for any injury to people or property resulting from any ideas, methods, instructions or products referred to in the content.